Provided for non-commercial research and education use.
Not for reproduction, distribution or commercial use.

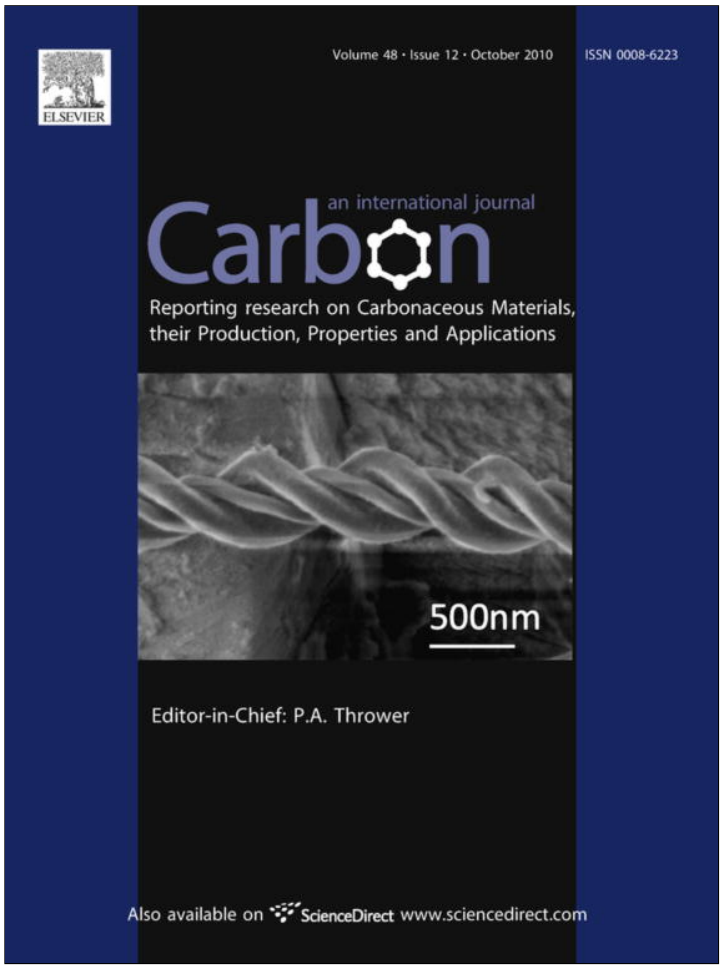

This article appeared in a journal published by Elsevier. The attached copy is furnished to the author for internal non-commercial research and education use, including for instruction at the authors institution and sharing with colleagues.

Other uses, including reproduction and distribution, or selling or licensing copies, or posting to personal, institutional or third party websites are prohibited.

In most cases authors are permitted to post their version of the article (e.g. in Word or Tex form) to their personal website or institutional repository. Authors requiring further information regarding Elsevier's archiving and manuscript policies are encouraged to visit:

http://www.elsevier.com/copyright

Author's personal copy

CARBON 48 (2010) 3382–3390

available at www.sciencedirect.com

ScienceDirect

journal homepage: www.elsevier.com/locate/carbon

Reduction of graphene oxide by electron beam generated plasmas produced in methane/argon mixtures

M. Baraket [a,*,1], S.G. Walton [a], Z. Wei [c,1], E.H. Lock [a,1], J.T. Robinson [b], P. Sheehan [c]

[a] Plasma Physics Division, Naval Research Laboratory, Washington, DC 20375, United States
[b] Electronics Division, Naval Research Laboratory, Washington, DC 20375, United States
[c] Chemistry Division, Naval Research Laboratory, Washington, DC 20375, United States

ARTICLE INFO

Article history:
Received 23 November 2009
Accepted 17 May 2010
Available online 25 May 2010

ABSTRACT

Graphene oxide (GO) was controllably reduced using electron beam generated plasmas produced in methane/argon mixtures. Operating parameters including, total pressure, duty factor (the ratio of the pulse duration to the pulse period), treatment time, and methane flow rate were varied to determine their impact on the reduction process. The resulting surface chemistry, topography and crystallinity of the reduced graphene oxide (r-GO) was determined with X-ray photoelectron spectroscopy (XPS), atomic force microscopy (AFM) and Raman spectroscopy. Oxygen concentration could be tuned to values between 43 at.% and 5 at.%, and under certain operating conditions the sp^2 cluster size grows. System diagnostics identified the critical operating parameters for the reduction of oxygen in GO.

Published by Elsevier Ltd.

1. Introduction

Graphene and graphene oxide have attracted considerable attention due to their potential applications in electronics [1,2], hydrogen storage [3–5] and more recently nano-biotechnology [6,7]. The unique properties of graphene, such as the exceptionally high electron mobility, mainly originate from its two-dimensional structure. Although multiple processes have been developed to grow graphene from heating SiC to mechanical cleavage of graphite, these approaches are exceptionally expensive due to either material or personnel costs and so appear to have limited industrial viability. An attractive alternative to graphene is graphene oxide (GO), which is prepared via oxidation of graphite [8–11] through protocols based on Hummers method [12]. GO is inexpensive to prepare, chemically flexible, and can be spun cast to form large area films. These films are a composite of individual GO flakes. Recently, it has been shown that flake size can be increased using microwave heating [8]. The hydroxyl, carboxyl, carbonyl and epoxide functional groups present on the basal surface or edge of graphene make it hydrophilic, and so it can even be dispersed in water instead of harsh solvents [9,13]. However, the presence of oxygen (or other functional groups) on the graphene sheets reduces electron mobility. Typically, graphene oxide is an insulator; however, when its oxygen concentration is reduced, its conductivity increases 4–5 orders of magnitude [14]. Thus, controlling the oxygen concentration in GO allows its electronic properties to be tuned for a wide variety of applications.

The reduction of graphene oxide has been carried out using wet chemistry approaches in both hydrazine hydrate (N_2H_4) [11] and sodium borohydride ($NaBH_4$) [15]. These treatments are time consuming (requiring up to 1 day). The preferred reducing agent N_2H_4, is toxic and can introduce nitrogen, which is undesirable for some applications. A plasma-based reduction process has been demonstrated by Gomez-Navarro et al. [16] using an RF-generated plasma discharge produced in high pressure (600 mTorr) hydrogen for 5–10 s. The plasma-reduced GO exhibited similar electronic properties to that of GO reduced in hydrazine hydrate.

In previous work [17], we have shown it is possible to reduce the oxygen concentration in GO using electron beam

* *Corresponding author:* Fax: +1 202 767 3553.
E-mail address: mira.baraket.ctr@nrl.navy.mil (M. Baraket).
[1] NRC/NRL postdoctoral associate.
0008-6223/$ - see front matter Published by Elsevier Ltd.
doi:10.1016/j.carbon.2010.05.031

Author's personal copy

generated plasmas produced in mixtures of argon and methane. In this work, we demonstrate a method to controllably reduce the amount of oxygen in graphene oxide films. Electron beam generated plasmas differ from conventional plasma discharges in that, while the plasma densities are high (10^{10}–10^{11} cm^{-3}), the electron temperatures are inherently low. This is due to the fact that plasma electrons are not heated by external electric fields and in molecular gases, the electrons are cooled to very low energies (<0.5 eV) via inelastic collisions [18]. This results in low plasma potentials and so ions impacting adjacent surfaces will do so with low kinetic energies (<3 eV) [18]. Small kinetic energies are critical for processing atomically thin materials such as graphene oxide since larger energies can significantly disrupt the film structure or etch the material away. Additionally, plasma-based techniques can be readily scaled up to industrially relevant processing rates.

2. Experimental

Fig. 1 is a schematic of the experimental whose details have been described previously [19]. Briefly, electron beam generated plasmas were produced by applying a −2 kV pulse to a linear hollow cathode. The electron beam produced by the hollow cathode passed through a slot in a grounded anode (slotted anode) and terminated at a second grounded anode (termination anode). The electron beam was confined by applying a magnetic field of 150 G with a Helmoltz coil located outside the chamber. The confinement of the electron beam resulted in a uniform sheet-like electron beam between the two anodes. The processing stage was located at 2.5 cm from the electron beam axis.

The base pressure (~10^{-7} Torr) in the chamber is maintained by a turbo molecular pump. Argon and methane were introduced through mass flow controllers and the desired operating pressures (25–100 mTorr) were achieved by reducing the pumping speed with a conductance limiter. A number of operating parameters (total pressure, duty factor, treatment time, and methane flow rate) were varied to determine their influence on the reduction process. When not varied, the parameter was held constant at an arbitrarily chosen "standard condition" summarized in Table 1. They are as follows: the pressure was 90 mTorr; the methane flow rate was 10% of the total flow rate (162 sccm Ar and 18 sccm CH_4); the duty factor was 10%, which is the ratio of the pulse width (2 ms) to the period (20 ms); and the treatment time was 30 s, which is the total time the plasma is on.

The graphene oxide was produced by the Hummers method [12] and dispersed in water by sonication. The solution was then spin cast on SiO_2 (300 nm)/Si substrates and then dried in nitrogen before placement in the vacuum chamber.

After plasma treatment, the reduced graphene oxide (r-GO) was subject to *ex situ* surface diagnostics, including X-ray photoelectron spectroscopy (XPS), Raman spectroscopy, and atomic force microscopy (AFM). For XPS (K-Alpha, Thermo Scientific), the chemical composition of the elements was identified using survey spectra and was quantified by integrating the area under the characteristic peak for each element. For much of this work, the chemical composition

Table 1 – Summary of the standard plasma operating conditions used in this work.

Parameter	Standard	Range
Pressure	90 mTorr	20–100 mTorr
Total flow rate	180 sccm	Fixed
Methane flow rate	18 sccm	0–36 sccm
Pulse width	2 ms	Fixed
Period	20 ms	5–40 ms
Duty factor	10%	5–40%
Treatment time	30 s	30–90 s

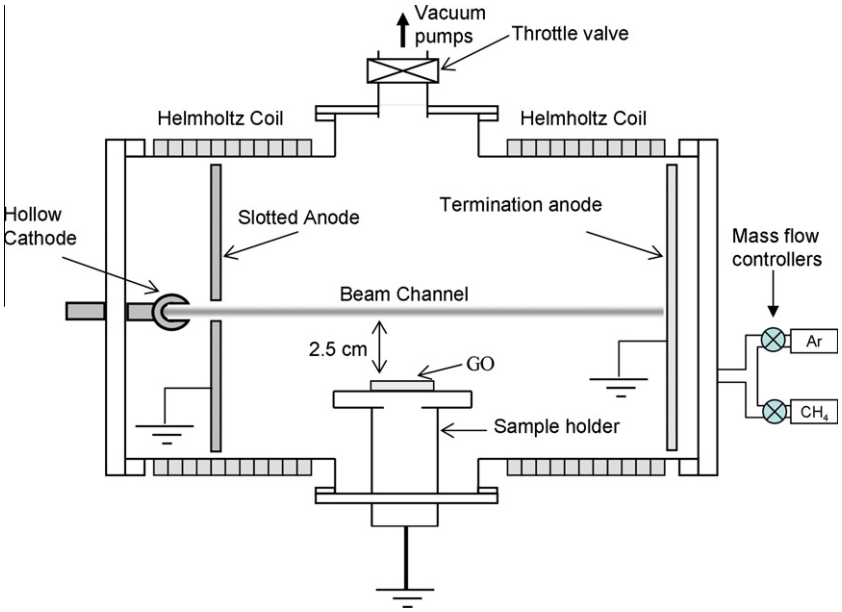

Fig. 1 – (Color online) A schematic of the experimental apparatus used to reduce GO.

Author's personal copy

will be presented as the oxygen concentration and the ratio of oxygen to carbon concentrations (O/C). The Raman characterization was performed using an InVia Raman microscope (Renishaw) equipped with a 50× objective with 514.5 nm diode laser excitation on 1800-line grating. The power was set to 20 mW at the source. The surface topography is examined by atomic force microscope (Nanoscope III, Veeco Metrology) on areas of $10 \times 10\ \mu m^2$.

3. Results

In this system, beam electrons are produced by ion-impact at the hollow cathode surface and so the beam current density will depend on the discharge density within the cathode. Thus, cathode current can be used as a general measure of beam current, which will, in turn, determine plasma generation and thus the reactive species fluxes at the graphene oxide surface and ultimately the reduction process. More succinctly, by varying the operating conditions we aim to control the oxygen concentration in GO. In Fig. 2, the hollow cathode current is shown as a function of the different operating parameters.

In Fig. 2a and b, a decrease of the hollow cathode current is observed while increasing the methane flow rate percentage (in the Ar/CH_4 gas mixture) and the duty factor, respectively. On the other hand, when the total pressure in the processing chamber increases, the hollow cathode current increases (Fig. 2c).

The changes in GO corresponding to the processing parameters in Fig. 2 are shown in Fig. 3. Here, the oxygen concentration of the reduced graphene oxide and the ratio of the oxygen to carbon concentrations (O/C) is presented. The O/C ratio of an untreated graphene oxide is 0.75 (≈43 at.% O_2). These results clearly show a dependence on the plasma operating parameters. Note that for all the plasma conditions used, except when pure argon was used or when the Ar/CH_4 mixture pressure was low (25 mTorr), the oxygen concentration in graphene oxide was significantly decreased.

Within each parameter range there are distinct trends, which provide the capability to regulate the oxygen concen-

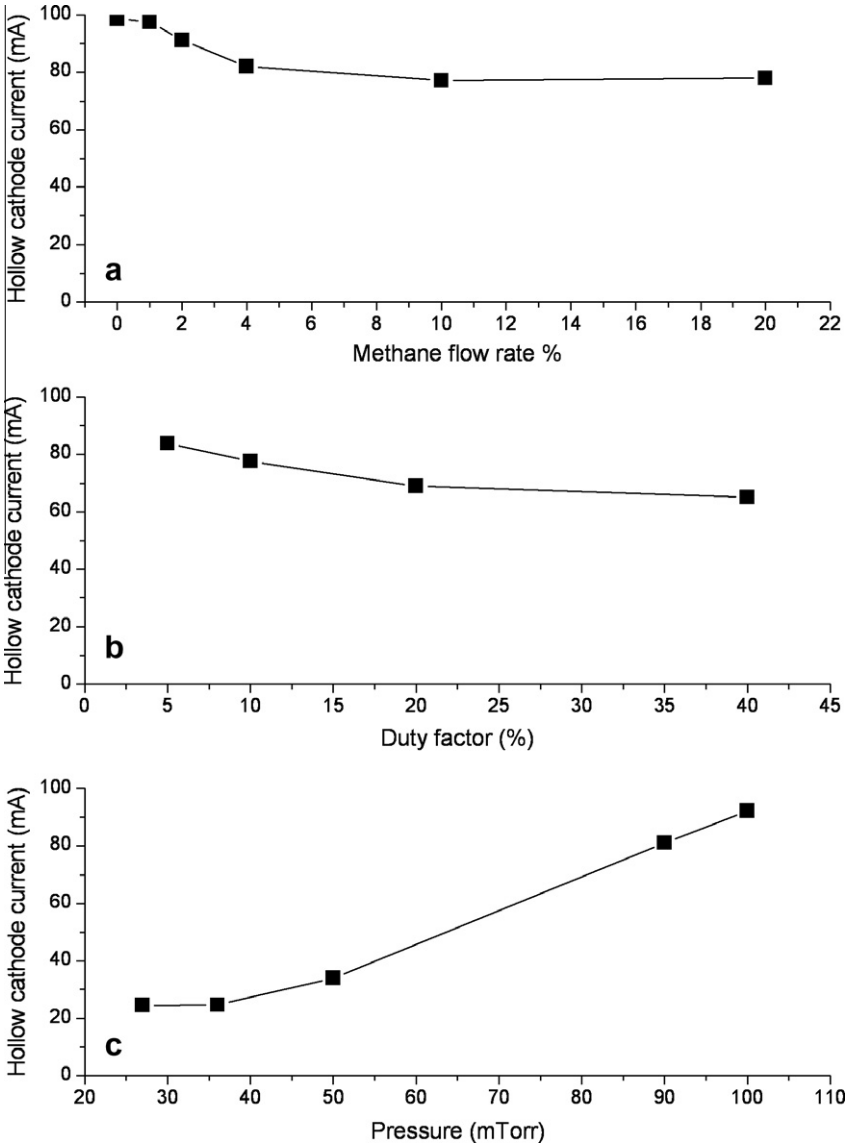

Fig. 2 – Hollow cathode current versus (a) methane flow rate percentage, (b) duty factor and (c) pressure.

Author's personal copy

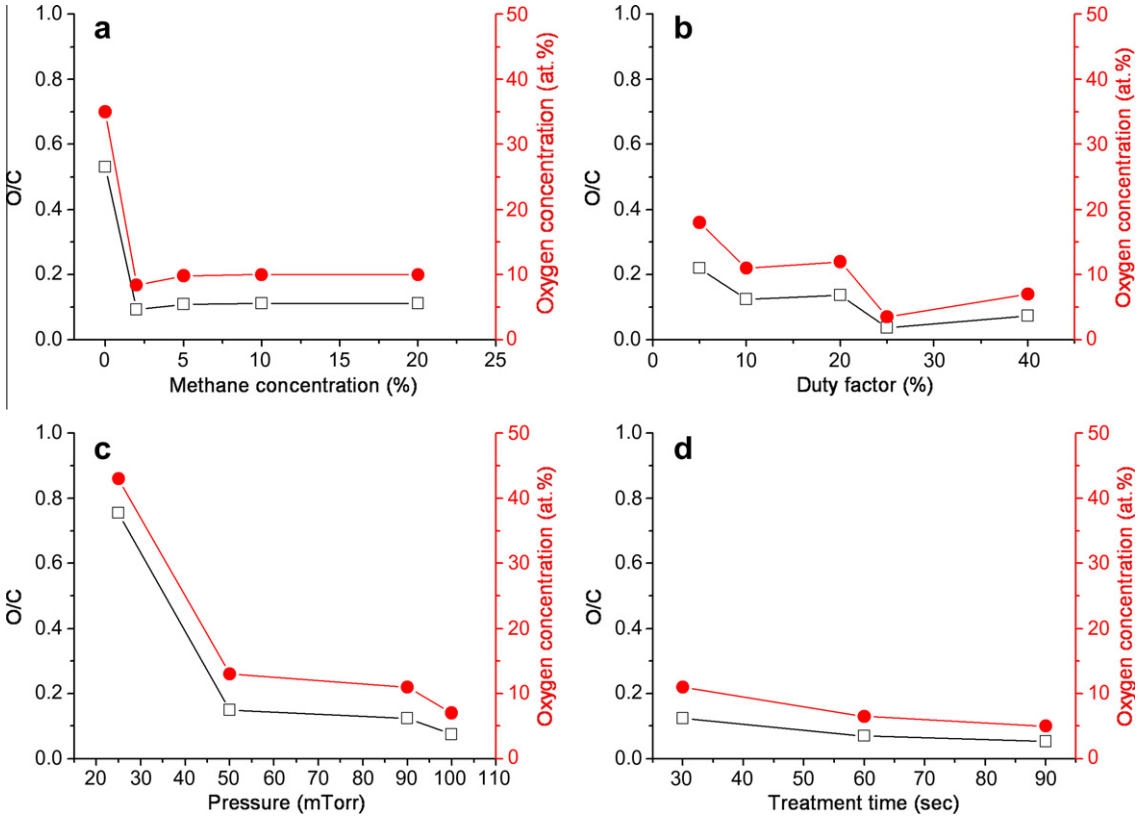

Fig. 3 – (Color online) O/C concentration ratio (open squares) and O concentration (filled circles) of the r-GO versus (a) methane flow rate percentage, (b) duty factor, (c) pressure and (d) treatment time.

tration between roughly 20 and 5 at.%. In Fig. 3a, the introduction of CH_4 causes a sharp decrease in the oxygen concentration. With a further increase in the CH_4 concentration (from 2% to 20% methane by flow), the oxygen concentration and thus the O/C ratio each increase by about 20%. Fig. 3b shows a decrease of the oxygen concentration with an increasing duty factor. At 5% duty factor, the O/C ratio was found to be 0.2 (≈18 at.% O_2) and non-uniformly decreases to about 0.075 (≈7 at.% O_2) at 40% duty factor. A large variation in the O/C ratio was found when the pressure was varied (Fig. 3c). At low pressure (25 mTorr), little change was observed but, with higher pressures (≥50 mTorr), the oxygen concentration decreases with increasing pressure. The O/C ratio was found to range from 0.2 (≈18 at.% O_2 at 50 mTorr) to 0.1 (≈9 at.% O_2 at 100 mtorr). Not surprisingly, the oxygen concentration was found to decrease with increasing treatment time, as shown in Fig. 3d.

In order to better understand the specifics of the reduction process, additional diagnostics and analyses were performed. The AFM images, presented in Fig. 4, shows the topography of unreduced GO (Fig. 4a), r-GO after a 30-s treatment (Fig. 4b), r-GO after a 90-s treatment (Fig. 4c), and r-GO treated for 90 s at a 40% duty factor (Fig. 4d). Also, shown in Fig. 4 are the AFM line scans and the corresponding GO/r-GO flake thicknesses (the scanned regions are represented by the white line in each figure).

Details of the C1s spectra are shown in Figs. 5 and 6. Fig. 5 shows the C1s high-resolution XPS spectra of the r-GO compared with that of unreduced GO (Fig. 5a). Fig. 5b and c shows the spectrum of r-GO after treatment times of 30 and 90 s, respectively. For comparison, the C1s spectra of pure graphene are shown in Fig. 5d. The high-resolution C1s XPS spectra presented in Fig. 6 shows the details of oxygen binding in unreduced GO and r-GO treated at the standard plasma conditions. The GO C1s spectrum was fitted to five components located at 284.4 eV (C–C), 286.5 eV (C–O), 287.6 eV (C═O), 288.8 eV (O–C═O) and 289.9 eV (π bond shake-up satellite). Note that no other elements besides carbon, oxygen and silicon (from the substrate) were observed by XPS for all samples.

Raman spectroscopy is sensitive to changes on the scales of a few Å and thus it is useful for the study of disorder in carbon films [20]. Raman spectra of the unreduced GO and its reduced counterpart produced using standard plasma conditions is presented in Fig. 7. The G band is observed around 1595 cm^{-1} and is attributed to the E2g phonon of C sp^2 atoms. The D band at 1350 cm^{-1} is attributed to the A1g mode activated by the presence of disorder [21]. Also distinguishable is the G′ band, an overtone of the G band [22], at 2700 cm^{-1} and the D + G combination mode at 2950 cm^{-1}. The ratio of D to G peak intensities is used to characterize the crystallinity of GO and r-GO samples.

4. Discussion

When the graphene oxide sample is exposed to Ar/CH_4 plasma, it will be subject to a flux of reactive species impinging on its surface. This flux is dependent upon the operating parameters and it includes ions (such as, Ar^+, H^+, CH_n^+ $n = 1$–5, and C^+), radicals (such as H and CH_n), and neutrals (such

Author's personal copy

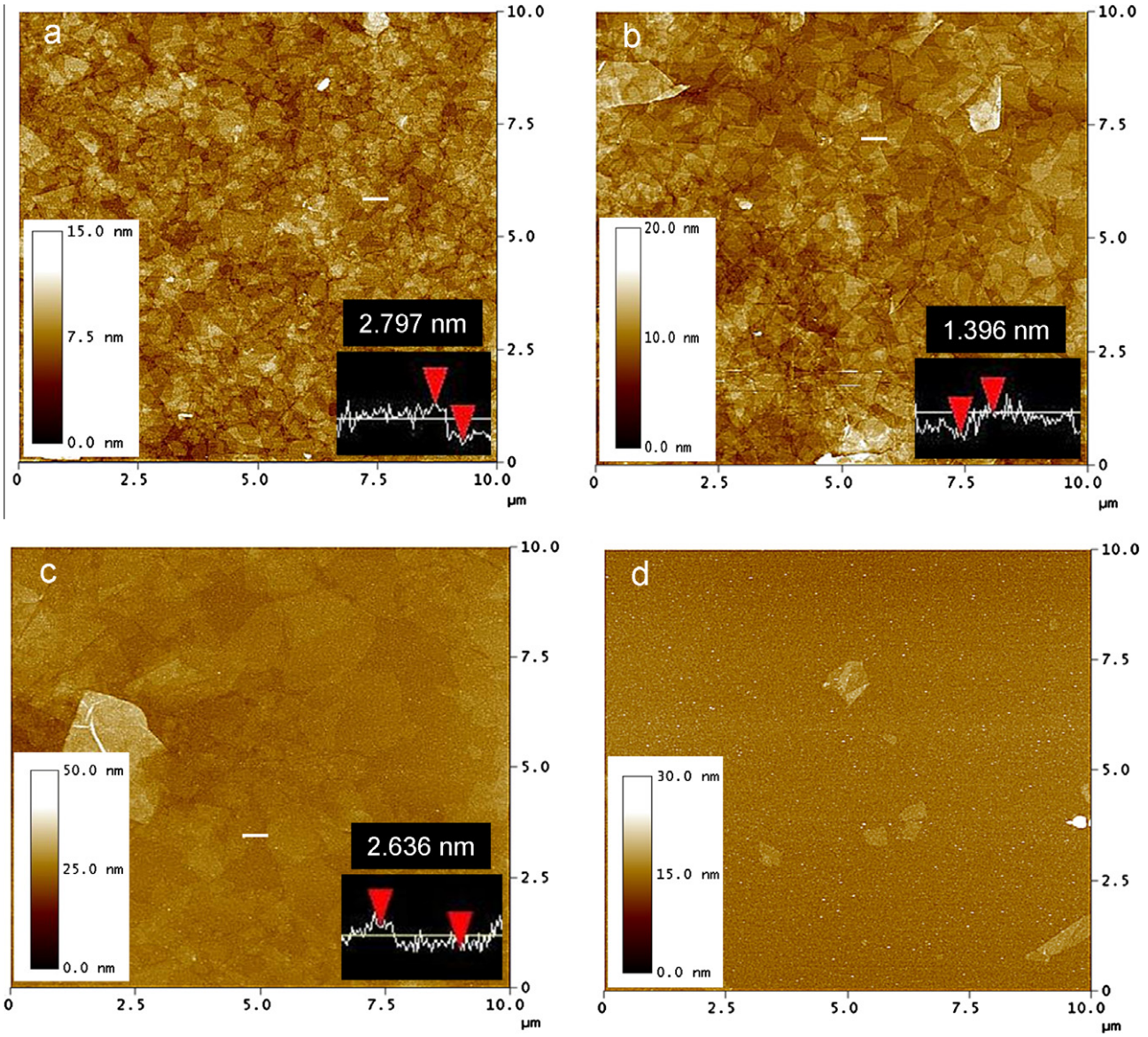

Fig. 4 – (Color online) AFM images of (a) unreduced GO, (b) r-GO after treatment time of 30 s, (c) r-GO after treatment time of 90 s, (d) r-GO after treatment time of 90 s at 40% duty factor. Also, shown are the AFM line scans and the corresponding GO/r-GO flake thicknesses.

as H_2). All species, except Ar, can react at the surface with oxygen to form volatile products (i.e., CO, OH, and H_2O) which can easily desorb from the surface, particularly under the influence of ion bombardment. Thus, a first order understanding of the production of species as a function of operating conditions is needed to understand the reduction process.

In electron beam produced plasmas, the production of ions and reactive species and thus their fluxes to adjacent surfaces is proportional to the electron beam current and the gas density (i.e., total pressure). Adapted from [23,24], the volumetric ionization rate of methane for electron beam generated plasmas produced in diluted methane is described by:

$$S = k \cdot D_f \cdot J_b \cdot P \cdot \left(\frac{f_{CH_4}}{f_{total}}\right) \cdot \sigma_i \quad (1)$$

where k is a constant, D_f is the duty factor, J_b is the beam current density which is proportional to the hollow cathode current, P is the total pressure, f_{CH_4}/f_{total} is the ratio of the methane flow rate to the total flow rate and σ_i is the ionization cross-section of any number of methane ionization channels [25], such as

$$e^- + CH_4 \rightarrow CH_4^+ + e^- \ (\sigma_i(1\ \text{keV}) = 4.76 \times 10^{-17}\ \text{cm}^2) \quad (2)$$

$$e^- + CH_4 \rightarrow CH_3^+ + H + e^- \ (\sigma_i(1\ \text{keV}) = 3.85 \times 10^{-17}\ \text{cm}^2) \quad (3)$$

$$e^- + CH_4 \rightarrow CH_2^+ + H_2 + e^- \ (\sigma_i\,(1\ \text{keV}) = 0.625 \times 10^{-17}\ \text{cm}^2) \quad (4)$$

It is important to note that the production of ions can be accompanied by the production of H (Eq. (3)) and/or H_2 (Eq. (4)).

Three of the parameters, duty factor, methane concentration, and pressure, varied in Figs. 2 and 3 will directly influence species generation in Eq. (1). The fourth, treatment time, obviously determines the exposure to these species. Consequently, the reduction of oxygen should have a depen-

Author's personal copy

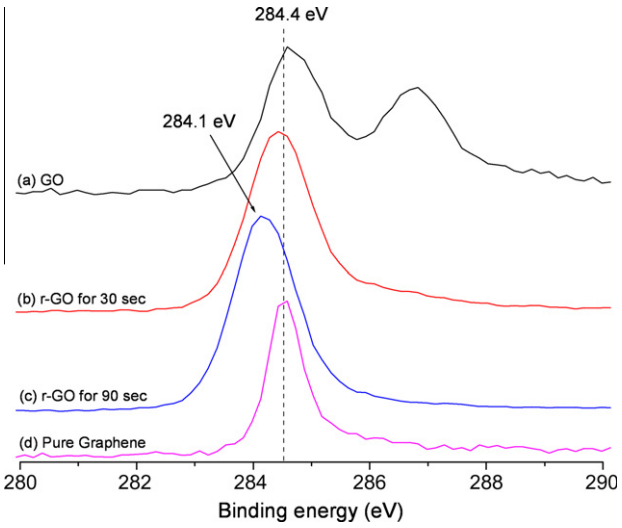

Fig. 5 – (Color online) C1s high-resolution XPS spectras of (a) unreduced graphene oxide, (b) r-GO for 30 s, (c) r-GO for 90 s and (d) pure graphene produced by CVD.

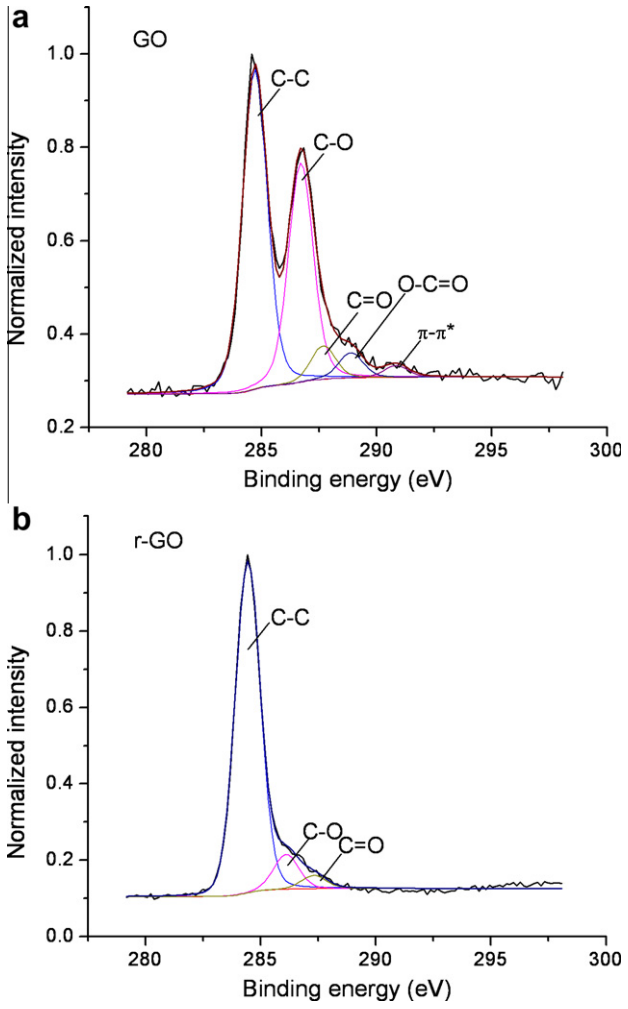

Fig. 6 – (Color online) High-resolution C1s spectra of (a) unreduced GO and (b) reduced GO treated at the standard conditions.

dency on the operating parameters. While a large decrease of the O/C ratio is observed under nearly all conditions, the variation was most notable when the pressure was varied.

In pure argon, a reduction in the oxygen concentration is observed, indicating that a flux of inert, low-energy ions is sufficient to remove oxygen. However, the addition of methane strongly increases the removal of oxygen. On the other hand, further increasing methane flow leads to an increase in oxygen. This may be explained by the overall decrease in plasma production (i.e., decrease in the hollow cathode current) associated with dissociative recombination (e.g., $CH_n^+ + e^- \rightarrow CH_{n-1} + H_n$), where plasma electrons and ions recombine to form neutral products. This process plays a major role in the neutralization of the argon/methane plasma. According to Sheehan and St.-Maurice [26], the dissociative recombination rate coefficients for the methane family ions (CH_n^+, n = 1–5) are $\sim 10^{-7}$ cm^3/s. Thus, the addition of methane, by increasing the relative flow rate, rapidly increases charge destruction leading to a decrease in the hollow cathode current (Fig. 2a) and the resulting beam current J_b in Eq. (1).

Also significant is the influence of recombination on the plasma chemistry in the electron beam produced plasma. Here, recombination strongly influences the charge density as the plasma diffuses from the beam region to the GO substrate, resulting in a decrease in the ion flux toward the GO surface and an increase in reactive neutral density (H, H_2, and CH_n). Both the beam current decrease and gas phase chemistry influence the oxygen concentration (and O/C ratio) as the methane flow is increased above a few percent in Fig. 3a. With an increasing duty factor, a decreasing cathode current is observed (Fig. 2b), which is characteristic of the circuit that powers the hollow cathode. However, since the electron beam generated plasma is operated at a larger duty factor (recall Eq. (1)), the graphene oxide films are subject to higher ion and reactive species flux per plasma period. Thus, a reduction in oxygen with increasing duty factor is observed in Fig. 3b.

The reduction in oxygen observed in Fig. 3c shows a strong dependence on the pressure. The larger gas density produces an increase of the hollow cathode current and thus the resulting beam current (Fig. 2c). From Eq. (1), an increase in both pressure and electron beam current increases the production and subsequent flux of plasma produced species at the surface. Thus, we see a considerable decrease of the O/C ratio from 0.75 (≈43 at.% O_2) for the r-GO treated at 25 mTorr to 0.075 (≈7 at.% O_2) at 100 mTorr. Here again, one should expect recombination to play a role since the change in ion flux will depend on both the plasma and neutral densities.

It is not surprising that increasing the treatment time leads to a decrease in the O/C ratio (Fig. 3c). Although, this decrease should be considered carefully since we have observed a different surface topography when the time exposure was 90 s. A smoothing of the surface is observed in the r-GO treated for 90 s (Fig. 4). Furthermore, a change in the C1s high-resolution spectra is observed in Fig. 5. The main carbon peak shifted from 284.4 eV for graphene and r-GO treated for 30 s toward lower binding energies (284.1 eV) when treatment time was 90 s, indicating the presence of disordered carbon species [27]. This is confirmed by the increase of the flakes average thickness to ≈2.6 nm (see line scan in Fig. 4c). One could also notice that for treatment times of 90 s when the

Author's personal copy

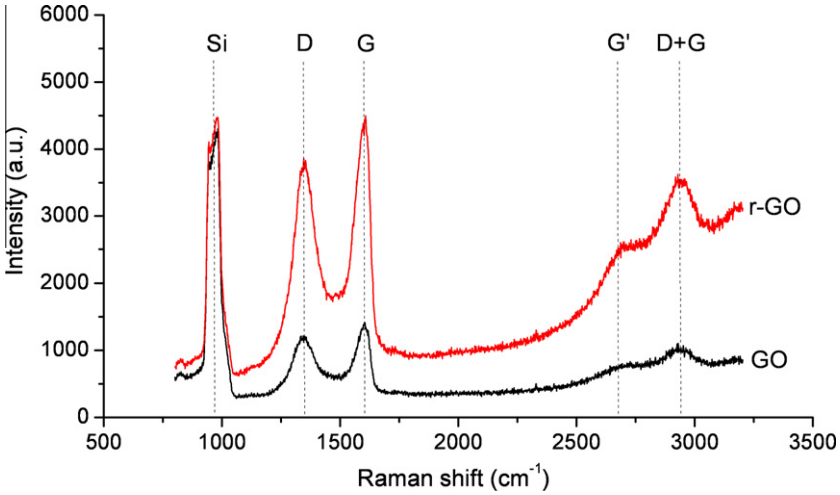

Fig. 7 – (Color online) Raman spectra of unreduced GO and the r-GO treated at the standard conditions.

duty factor was increased to 40%, a flat surface with only few flakes is observed (Fig. 4d). The surface does not appear to have been etched away since carbon with 5% of oxygen was still observed via XPS analysis. These results suggest not only amorphous carbon deposition but also a kind of selective deposition; that is, deposition seems to occur between the GO flakes rather than a uniform deposition over the entire surface.

Importantly, the treatment at standard conditions does not lead to noticeable deposition of carbon, which is verified by AFM where a surface topography similar to that of graphene oxide without treatment (see Fig. 4a and b) was observed. In addition, no shift of the main C1s XPS peak (C–C) toward lower binding energies was observed (see Fig. 5) and the r-GO flakes thickness decreases (see line scans in Fig. 4b). The XPS high-resolution C1s spectra (normalized to the maximum intensity) of r-GO at the standard conditions is compared to the unreduced GO in Fig. 6. The reduced GO displays a significant decrease of the oxidized carbon components. The O–C=O peak is completely absent and the C–O and C=O peaks accounted for only 9% and 4% of the C1s spectra area instead of 37% and 7%, respectively, in the case of unreduced GO. The contribution (area percentage) of each component of the C1s spectra of GO and r-GO is presented in Table 2.

From the Raman spectra in Fig. 7, the ratio of G to D peak intensities I_D/I_G of the untreated GO varies between 0.9 and 1 while in r-GO, the ratio varies between 0.7 and 1. By comparison, when the hydrazine hydrate was used to reduce GO, the ratio was higher after reduction. This was attributed to the decrease of the sp^2 in-plane domain [11, 28] induced by the creation of defects, vacancies and distortions of the sp^2 domains [29], which are due to the removal of oxygen from the graphene sheet. In our case, ratio values before and after reduction are essentially the same, suggesting the vacancies created by the evacuation of oxygen were somehow "healed", perhaps replaced by carbon atoms formed on the surface by dissociation of CH_n neutrals and ions.

It should be noted that the D peak of the graphene structure is not only present because of the oxygen impurities and vacancies but also due to the film structure. It has been reported [30] that edges of graphene are always seen as defects, and so the D peak could also have contributions from the non-uniformity, corrugation, and twisting in the graphene flakes. For the Raman spectroscopy, the spot size is estimated to be 3–5 μm in diameter and such an area would contain a high percentage of edges and irregular graphene flakes (see AFM image in Fig. 4).

Table 2 – Area % contribution of each component of the C1s high-resolution spectra of GO and r-GO at the standard conditions.

	% C–C	% C–O	% C=O	% O–C=O
GO	54	37	7	4
r-GO	87	9	4	0

Tuinstra and Koenig [21] developed an empirical formula relating the sp^2 cluster size (La) to the ratio of the intensity of the D and G peaks:

$$\mathrm{La\,(nm)} = \frac{10^3}{227 \cdot \left(\frac{I_D}{I_G}\right)}$$

The average cluster size of our GO is evaluated to 4.6 nm before plasma treatment and increases to 5.2 nm after treatment at the standard plasma conditions. This is in contrast to chemically reduced graphene oxide, where the sp^2 cluster size decreased from ≈3.5 nm to ≈3 nm (calculated from [31]) and thermally reduced GO, where the cluster size is reduced from ≈3.5 nm to ≈3.15 nm (calculated from [31]) or slightly increased from 2.5 nm to 2.8 nm [32]. In this work, the reduction of oxygen in GO generates an expansion of the spatial distribution of the sp^2 phase. Further evidence of the removal of oxygen without etching the graphene film is observed by the decrease in the GO flake thickness from around 2.8 nm for pristine GO to around 1.4 nm for r-GO at the standard conditions (see AFM line scans presented in Fig. 4a and b), which is similar to that found for chemically reduced graphene [33] or for graphene obtained by mechanical cleavage [34]. This result demonstrates that our plasma-based technique is a viable technique to reduce GO to graphene-like films without

Author's personal copy

damaging their graphitic structure. This is made possible by the low incident ion energies provided by the electron beam generated plasmas. In this work, the mean ion energy is about 3 eV and is lower than the bonding energy of the C–C (3.61 eV), C=C (6.35 eV), C–O (3.72 eV), C=O (7.7–8.35 eV) bonds that form graphene oxide. The ion energies are low enough that no significant etching occurs but high enough to produce ion-stimulated oxygen removal, preferably by desorption of weakly bonded oxygen-containing groups.

5. Summary

This work demonstrates a controlled reduction in the oxygen concentration in graphene oxide using electron beam generated plasmas produced in gas mixtures of argon and methane. Oxygen concentrations were varied between 43 at.% and 5 at.% depending on the plasma operating parameters. The desired oxygen concentration/operating parameter should be chosen carefully to achieve a reduced GO similar to the starting material (with intact graphene flakes) and to prevent over treatment. The operating pressure provided the best control over oxygen concentration.

The results of simple plasma diagnostics were used to correlate the production of reactive plasma species to the reduction of oxygen. The reduction in pure argon showed that a flux of inert, low-energy ions is sufficient to reduce the oxygen on the surface. The addition of methane further reduces the oxygen concentration indicating that the presence of reactive species (CH_n or H) produces volatile oxygen-containing components that provide a pathway for oxygen removal. Also, the presence of reactive CH_n species likely helps reduce the amount of defects, associated with the removal of oxygen from the surface commonly observed through chemical reduction approaches, by adding carbon. Moreover, the presence of carbon species plays a key role in increasing of the sp^2 phase cluster size observed upon reduction. Further experiments are in progress to better understand the mechanism that drives the reduction process.

Acknowledgement

This research was supported by the Office of Naval Research. M.B., E.H.L. and Z.W. appreciates the support of the National Research Council. Dr. J. Butler from NRL is gratefully acknowledged for the use of Raman Spectrometer.

REFERENCES

[1] Wang ZF, Zheng H, Shi QW, Chen J. Emerging nanodevice paradigm: graphene based electronics for nanoscale computing. ACM J Emerg Technol Comput Syst 2009;5(1):1–19.
[2] Eda G, Fanchini G, Chhowalla M. Large-area ultrathin films of reduced graphene oxide as a transparent and flexible electronic material. Nat Nanotechnol 2008;3:270–4.
[3] Elias DC, Nair RR, Mohiuddin MG, Morozov SV, Blake P, Halsall MP, et al. Control of graphene's properties by reversible hydrogenation: evidence for graphane. Science 2009;323:610–3.
[4] Strobel R, Garche J, Moseley PT, Jorissen L, Wolf G. Hydrogen storage by carbon materials. J Power Sour 2006;159:781–801.
[5] Sofo JO, Chaudhari AS, Barber GD. Graphane: a two-dimensional hydrocarbon. Phys Rev B 2007;75(153401):1–4.
[6] Chopra N, Bachas LG, Knecht MR. Fabrication and biofunctionalization of carbon-encapsulated Au nanoparticles. Chem Mater 2009;21:1176–8.
[7] Shan C, Yang H, Song J, Han D, Ivaska A, Niu L. Direct electrochemistry of glucose oxidase and biosensing for glucose based on graphene. Anal Chem 2009;81:2378–82.
[8] Luo Z, Lu Y, Somers LA, Charlie Johnson AT. High yield preparation of macroscopic graphene oxide membranes. J Am Chem Soc 2009;131:898.
[9] Stankovich S, Dikin A, Dommett GHB, Kohlhaas KM, Zimney EJ, Stach EA, et al. Graphene-based composite materials. Nature 2006;442:282–6.
[10] Wei Zhongqing, Barlow Daniel E, Sheehan Paul E. The assembly of single-layer graphene oxide and graphene using molecular templates. Nano Lett 2008;8(10):3141–5.
[11] Stankovich S, Dinkin D, Piner RD, Kohlhaas KA, Kleinhammes A, Jia Y, et al. Synthesis of graphene-based nanosheets via chemical reduction of exfoliated graphite oxide. Carbon 2007;45:1558–65.
[12] Hummers Jr WS, Offeman RE. Preparation of graphitic oxide. J Am Chem Soc 1958;80:1339.
[13] Wang G, Wang B, Park J, Yang J, Shen X, Yao J. Synthesis of enhanced hydrophilic and hydrophobic graphene oxide nanosheets by a solvothermal method. Carbon 2009;47:68–72.
[14] Jung I, Dikin D, Park S, Cai W, Mielke SL, Ruoff RS. Effect of water vapor on electrical properties of individual reduced graphene oxide sheets. J Phys Chem C 2008;112:20264–8.
[15] Shin HJ, Kim KK, Benayad A, Yoon SM, Park HK, Jung IS, et al. Efficient reduction of graphite oxide by sodium borohydride and its effect on electrical conductance. Adv Funct Mater 2009;19:1987–92.
[16] Gomez-Navarro C, Weitz RT, Bittner AM, Scolari M, Mews A, Burghard M, et al. Electronic transport properties of individual chemically reduced graphene oxide sheets. Nano Lett 2007;7:3499–503.
[17] Walton SG, Lock EH, Baraket M, Sheehan PE, Wei Z, Robinson JT, et al. Plasma-based approach to controlling the oxygen concentration in graphene oxide. In: Proceedings, 52nd SVC Annual Technical Conference. Santa Clara, California, USA. Society of Vacuum Coaters; 2009. p. 4.
[18] Walton SG, Muratore C, Leonhardt D, Fernsler RF, Blackwell DD, Meger RA. Electron-beam-generated plasmas for materials processing. Surf Coat Technol 2004;186:40–6.
[19] Leonhardt D, Walton SG, Fernsler RF. Fundamentals and applications of a plasma-processing system based on electron-beam ionization. Phys Plasmas 2007;14(057103):1–7.
[20] Lespade P, Al-Jishi R, Dresselhaus MS. Model for Raman scattering from incompletly graphetized carbons. Carbon 1982;20:427–31.
[21] Tuinstra F, Koenig JL. Raman spectrum of graphite. J Chem Phys 1970;53:1126–30.
[22] Park JS, Reina A, Saito R, Kong J, Dresselhaus G, Dresselhaus MS. G′ band Raman spectra of single, double and triple layer graphene. Carbon 2009;47:1303–10.
[23] Manheimer WM, Fernsler RF, Lampe M, Meger RA. Theoretical overview of the large-area plasma processing system (LAPPS). Plasma Sour Sci Technol 2009;9:370–86.
[24] Walton SG, Lock EH, Ni A, Baraket M, Fernsler RF, et al. Study of plasma-polyethylene interactions using electron beam generated plasmas produced in Ar/SF6 mixtures. J Appl Polym Sci 2010;117:3515–23.
[25] Straub HC, Lin D, Lindsay BG, Smith KA, Stebbings RF. Absolute partial cross sections for electron-impact ionization

Author's personal copy

of CH_4 from threshold to 1000 eV. J Chem Phys 1997;106:4430–5.
[26] Sheehan CH, St.-Maurice JP. Dissociative recombination of the methane family ions: rate coefficients and implications. Adv Space Res 2004;33:216–20.
[27] Rodriguez NM, Anderson PE, Wootsch A, Wild U, Schlogl R, Paal Z. XPS, EM and catalytic studies of the accumulation of carbon on Pt black. J Catal 2001;197:365–77.
[28] Wang G, Yang J, Park J, Gou X, Wang B, Liu H, et al. Facile synthesis and characterization of graphene nanosheets. J Phys Chem C 2008;112:8192–5.
[29] Yuan GD, Zhang WJ, Yang Y, Tang YB, Li YQ, Wang JX, et al. Graphene sheets via microwave chemical vapor deposition. Chem Phys Lett 2009;467:361–4.
[30] Ferrari AC. Raman spectroscopy of graphene and graphite: disorder, electron-phonon coupling, doping and nonadiabatic effects. Solid State Commun 2007;143:47–57.
[31] Cuong TV, Pham VH, Tran OT, Hahn SH, Chung JS, et al. Photoluminescence and Raman studies of graphene thin films prepared by reduction of graphene oxide. Mater Lett 2010;64:399–401.
[32] Mattevi C, Eda G, Agnoli S, Miller S, Mkhoyan A, et al. Evolution of electrical, chemical, and structural properties of transparent and conducting chemically derived graphene thin films. Adv Funct Mater 2009;19:2577–83.
[33] Zhang T, Zhang D, Shen M. A low-cost method for preliminary separation of reduced graphene oxide nanosheets. Mater Lett 2009;63:2051–4.
[34] Nemes-Incze P, Osvath Z, Kamaras K, Biro LP. Anomalies in thickness measurements of graphene and few layer graphite crystals by tapping mode atomic force microscopy. Carbon 2008;46:1435–42.